AGU PUBLICATIONS

JGR

Journal of Geophysical Research: Atmospheres

RESEARCH ARTICLE
10.1002/2013JD020326

Key Points:
- Quasi-Lagrangian measurements of polar stratospheric cloud particles
- Balloon-borne measurements of nitric acid trihydrate formation

Correspondence to:
S. M. Ward,
sward7@uwyo.edu

Citation:
Ward, S. M., T. Deshler, and A. Hertzog (2014), Quasi-Lagrangian measurements of nitric acid trihydrate formation over Antarctica, *J. Geophys. Res. Atmos.*, *119*, 245–258, doi:10.1002/2013JD020326.

Received 7 JUN 2013
Accepted 10 DEC 2013
Accepted article online 13 DEC 2013
Published online 15 JAN 2014

Quasi-Lagrangian measurements of nitric acid trihydrate formation over Antarctica

Shauna M. Ward[1], Terry Deshler[1], and Albert Hertzog[2]

[1]Department of Atmospheric Science, University of Wyoming, Laramie, Wyoming, USA, [2]Laboratoire de Météorologie Dynamique, Ecole Polytechnique, Palaiseau, France

Abstract In 2010, the joint French-United States Concordiasi project released 19 long-duration superpressure balloons from McMurdo Station, Antarctica. Four of these balloons carried a gondola with particle counters and temperature sensors to measure polar stratospheric clouds. One gondola spent 5 days at stable temperatures between equilibrium temperatures for nitric acid trihydrate (NAT) and for supercooled ternary solution droplets. Sporadic particles with radii between 0.46 μm and 4.5 μm were measured in a small fraction of the measurements. At these times the corresponding size distributions and total particle volumes were consistent with NAT. Although the fraction of these observations was less than 3%, their frequency increased with time over the 5 days. From this frequency the NAT nucleation rate at 3°C below T_{NAT} was estimated to be $2 \times 10^{-4}\,m^{-3}\,s^{-1} \pm 60\%$ for these late winter austral NAT observations at a potential temperature of 410–415 K. Interspersed with these measurements of polar stratospheric cloud particles consistent with NAT were many more measurements of particles consistent with background stratospheric aerosol indicating that the polar stratospheric clouds sampled were highly discontinuous.

1. Introduction

Polar stratospheric clouds (PSCs) have been observed over the poles dating back to the 1870s [*Stanford and Davis*, 1974] and were a puzzle in satellite observation in the early 1980s [*McCormick et al.*, 1982]; however, significant research regarding these clouds was sparked with the discovery of their relationship to ozone depletion [*Farman et al.*, 1985; *Solomon et al.*, 1986; *Hofmann et al.*, 1987]. Subsequent theoretical considerations [*Crutzen and Arnold*, 1986; *Toon et al.*, 1986] suggested that PSC particles contain nitric acid and water, while lidar observations showed two growth modes for PSCs, one above the frost point, T_{ICE}, and one below [*Poole and McCormick*, 1988]. Particles existing above T_{ICE} were believed to consist of nitric acid trihydrate (NAT) [*Hanson and Mauersberger*, 1988; *Pueschel et al.*, 1989] and those below T_{ICE} as ice. *Dye et al.* [1990] compared model volumes of NAT and ice to aircraft measurements and found many cases when the particle concentration measurements were not consistent with either NAT or ice. This led to the identification of an intermediate solution droplet of sulfuric acid, nitric acid, and water, now referred to primarily as supercooled ternary solutions (STSs) [*Dye et al.*, 1992; *Carslaw et al.*, 1994; *Tabazadeh et al.*, 1994], although occasionally as liquid ternary aerosol.

Field observations by a balloon-borne mass spectrometer provided the first direct measurements of NAT particles within a PSC [*Voigt et al.*, 2000; *Schreiner et al.*, 2003]; however, NAT has not been found in many observations at temperatures below the NAT point in the Arctic [*Poole et al.*, 1988; *Deshler et al.*, 2000] and Antarctic [*Dye et al.*, 1996; *Del Negro et al.*, 1997], indicating the presence of a nucleation barrier [*Zhang et al.*, 1996; *Koop et al.*, 1997]. Suggestions of the presence of a nucleation barrier for NAT and the consequences for the vertical extent of denitrification were also illustrated with the observations of very large NAT particles by *Fahey et al.* [2001]. Laboratory measurements have required temperatures below T_{ICE} for NAT to form [*Middlebrook et al.*, 1993; *Koop et al.*, 1995]. Some field measurements are consistent with an ice-based nucleation mechanism [*Carslaw et al.*, 1998; *Tabazadeh et al.*, 1994], and models have assumed an ice mother cloud as the source of large NAT particles [*Fueglistaler et al.*, 2002], which is consistent with some observations [*Pitts et al.*, 2011]. Other field observations, coupled with temperature histories, however, show that there also must be a non-ice nucleation mechanism for NAT formation [*Larsen et al.*, 1997; *Deshler et al.*, 2003a]. Assuming NAT does not require temperatures below T_{ICE} to nucleate, the rate of this nucleation has been modeled to match observations [*Voigt et al.*, 2005; *Davies et al.*, 2005; *Larsen et al.*, 2004; *Grooβ et al.*, 2005; *Tabazadeh et al.*, 2001].

The following shows the first measured NAT nucleation rate by in situ particle measurements from a balloon-borne gondola floating in an air parcel. These quasi-Lagrangian measurements observed, sporadically, particles greater than 1 μm radius that had been initiated, without temperatures cooling below T_{ICE} after an extended time period below T_{NAT}.

2. Project/Instrumentation

In 2010, the joint French-United States Concordiasi project completed its final set of field measurements with the release of 19 long-duration superpressure balloons from McMurdo Station, Antarctica [*Rabier et al*., 2013]. Thirteen balloon gondolas contained 50 pressure, temperature, and humidity sondes which were dropped on demand for comparison with nearly simultaneous satellite observations, particularly in regions where satellite retrievals of the state parameters have difficulty. Six carried in situ instruments to measure ozone, while four of these also carried particle counters. The four particle instruments were Wyoming laser particle counters (WLPCs) to measure stratospheric particle size distributions. Each gondola also carried a GPS receiver to measure balloon position (from which the wind is deduced) and a meteorological package (called "Tsen") to measure temperature and pressure [*Hertzog et al*., 2007].

Specifically, temperature is measured by two 130 μm diameter thermistors located 7 m below all other instrumentation. This distance was established by previous test flights showing this distance to be sufficient to escape the majority of gondola or balloon influence. *Boccara et al*. [2008] have shown a good agreement between previous superpressure balloon and analyzed temperatures over Antarctica, except for small-scale motions, e.g., gravity waves, which are not resolved by models. The thermistors are exposed to solar radiation creating ~1°C warm bias during the day. This warm bias was corrected by comparing systematic differences between daytime and nighttime measurements [*Hertzog et al*., 2004]. The precision of the thermistor measurement was found to be 0.25°C, the standard deviation of the distribution of temperature differences for each gondola thermistor pairs over all Concordiasi flights. The temperature used for analysis of a single gondola is the mean of the two measurements at each sampling time.

The white light optical particle counters (OPCs) typically flown on sounding balloons in the midlatitudes and polar regions by the University of Wyoming [*Deshler et al*., 2003a, 2003b] could not be used on the long-duration balloons due to temperature sensitivity and limited lamp lifetimes. The WLPC, which was developed by Particle Metrics Inc., Boulder, Colorado, and modified for atmospheric aerosol measurements by the University of Wyoming, has been flown from Laramie, Wyoming, in comparison with the white light OPCs [*Glen*, 2007]. The Laramie measurements have primarily transitioned to the WLPC, based on the reasonable agreement between the new and older instrument. Although not initially developed for long-duration ballooning, the WLPC could be adapted, without major modification to the sampling method, to this harsher sampling environment, requiring limited power consumption and ability to start at −40°C after cold soaking.

Although in principle the WLPC is quite similar to the OPC, there are some differences, which will be described here as this is the first introduction of this instrument into the literature, aside from the thesis of *Glen* [2007]. Within the WLPC particles are drawn through a straight inlet into an open cavity laser. Small particles in the laser cavity are sensed through collection of side-scattered light, larger particles through the extinction of the forward laser beam. Instruments were calibrated to measure particles in eight channels with size thresholds at 0.075, 0.15, 0.25, 0.5, 1.0, 2.5, 5.0, and 15.0 μm radii, extending the measurement range of the older OPCs in both directions. All particle sizes are given in radius. For the measurement presented here the flow rate is 10 L/min, sampling frequency is 0.1 Hz, and the sizing uncertainty is ± 10%. These physical characteristics are quite similar to the OPCs described by *Deshler et al*. [2003b], and thus, minimum detectable concentrations, concentration uncertainties due to Poisson counting statistics, and uncertainties of particle size distribution moments are the same as for the OPC. Minimum detectable concentrations are 6×10^{-4} cm^{-3}, uncertainties in concentration are 85, 25, and 8% for concentrations of 0.001, 0.01, and 0.1 cm^{-3}, and uncertainties of ± 40% apply to distribution moments from the WLPC measurements.

Power on the Concordiasi gondola was provided by batteries recharged with solar cells. The WLPC draws 30 W; thus, for the long-duration balloon flights the WLPC was designed to take measurements for 15 min when first turned on, and then to sample for 2 min of every 15 min thereafter. The WLPC could be turned off in regions void of PSCs to extend instrument lifetime, which was limited to 20–30 h of operation due to wear on the gears

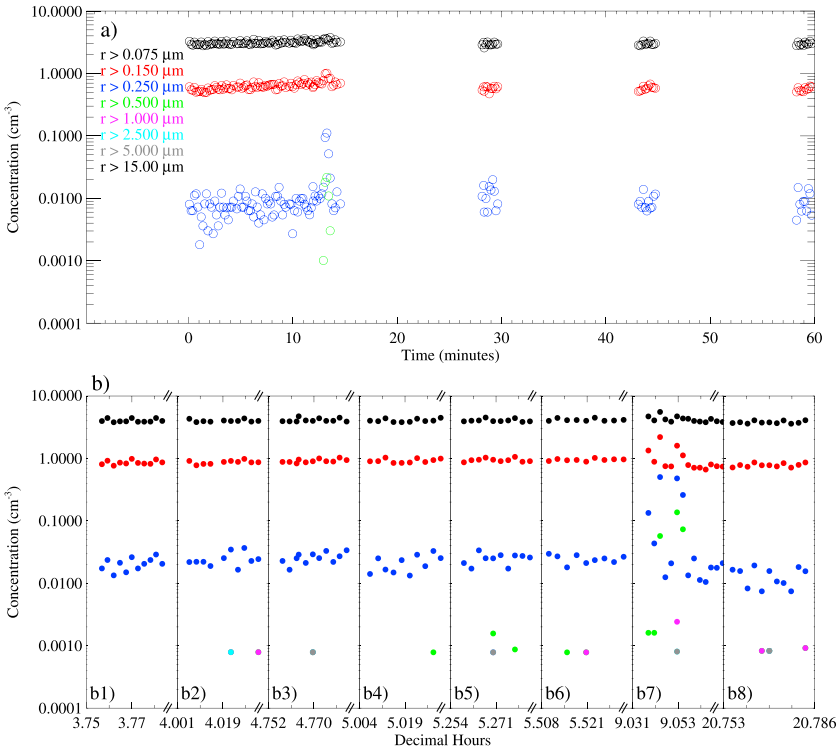

Figure 1. Measurements of number concentration from the WLPC. (a) Time in minutes versus number concentration. Each open circle represents a 10 s measurement in a different size channel, with channel boundary indicated in the upper left. (b) Eight random 2 min samples from the WLPC flight on 12 September. Colors for different size channels are the same as those listed in the upper left of Figure 1a.

of the constant volume gear pump. Due to logistical constraints and temperatures experienced during this flight, the WLPC was left turned on, sampling for 2 of every 15 min period nearly throughout the flight. An example hour of WLPC measurement is shown in Figure 1a as the instrument was turned on for that day, showing the initial 15 min and then each subsequent 2 min sample. Particles < 0.25 μm were measured throughout with one short period with particles in the larger channels. The concentration remained consistent for particles at the two smallest sizes, indicating consistency from one measurement to the next. This consistency indicates that the intermittent data collection technique was equivalent to obtaining 2 min samples from one continuous sample. Aside from saving instrument power, the intermittent sampling limited self-contamination of the measurements from instrument exhaust as the balloon drifted with the air parcel, since at least all initial measurements in a 2 min sample would be free from such exhaust. The WLPC was only sampling for 13% of the flight time, and the exhaust was separated from the intake by 0.5 m. Implicit in the measurements is the assumption that the particle environment around the gondola was not influenced by the gondola nor by the exhaust from the WLPC. There is no way to confirm this. The fact that in the 2 min sampling period the measured concentrations were nearly static and that large particle observations were scattered randomly within that period, Figure 1b is suggestive that the WLPC exhaust is not causing a bias.

Eight 2 min samples, irregularly distributed throughout the day on 12 September of the WLPC flight when temperatures were below T_{NAT}, are shown in Figure 1b. These samples also show, throughout the day, highly consistent measurements for particles < 0.25 μm. Measurements of particles larger than 0.50 μm and up to 5.0 μm appear randomly within most 2 min sample periods.

Due to the unpredictability of the long-duration balloon flight paths and the inaccessibility of landing locations, the return of the WLPCs after flight was considered highly unlikely. Fortunately, luck was on the side of science. Three of the four WLPCs were recovered. The first WLPC released from McMurdo had an instrument command module that failed after 6 days; however, the balloon continued around the vortex passing near McMurdo where it was cut down after 8 days of flight. The instrument then remained on the ice for a month until it could be recovered by helicopter. Another WLPC flew for about a month before being similarly cut

down near McMurdo and retrieved. The third WLPC flew for over 2 months before it was cut down over Tasmania, Australia, in December and recovered. The fourth instrument failed prior to making any useful measurements and was lost.

After returning from Antarctica, postflight tests were performed to check the channel size boundaries on all three recovered instruments. These tests indicated that the channel boundaries were at the expected sizes within ± 20% between preflight calibrations and postflight tests. These results seem quite reasonable considering the harshness of the conditions experienced by the WLPCs. In spite of the lucky recoveries, and the positive postflight checks, there were either serious in-flight problems, or the instruments did not manage to sample microphysically interesting temperature environments, for the second and third WLPC flights. Thus, the focus of analysis here is on the first WLPC which was released late on 8 September and reached its ceiling in an air parcel at temperatures warmer than T_{NAT}. The air parcel then cooled to remain at temperatures between T_{NAT} and the temperature when STS would be expected, until the command module failed on 14 September. Postflight tests of this WLPC indicated size boundaries at 0.085, 0.13, 0.25, 0.46, 1.20, 2.50, 4.50, and 12.0 μm and the nominal size uncertainty of ± 10%. Assuming no internal changes to the instrument due to landing or transport back to Wyoming, the postflight sizes will be assumed for the flight.

Mixing ratios of HNO_3 and H_2O were obtained from the Microwave Limb Sounder (MLS) on the Aura satellite from the day before the flight through the flight. These mixing ratios showed little longitudinal or temporal variation over the period but did show a slight latitudinal decrease toward the South Pole. Considering this, the quasi-Lagrangian nature of the measurements, and a lack of evidence of significant particle sedimentation during the measurements, average MLS mixing ratios for both HNO_3 and H_2O were used for the PSC analysis. The average was constructed from the ensemble of zonal mixing ratios matching the gondola trajectory, thus weighting the average to the dominant latitudes during the flight. MLS measurement uncertainties are ± 0.7 ppbv for HNO_3 and ± 15% for H_2O [*Livesey et al*., 2011]. The standard deviation of the averages used for the flight are less than the uncertainty of the HNO_3 measurement and similar to the uncertainty of the H_2O measurement.

Using HNO_3 and H_2O mixing ratios, as well as an H_2SO_4 mixing ratio determined from background particle measurements, equilibrium temperatures for ice [*Marti and Mauersberger*, 1993] and for NAT [*Hanson and Mauersberger*, 1988] were calculated. An STS threshold temperature, T_{STS}, was defined, following *Deshler et al*. [2003a], as the temperature at which the liquid particle volume [*Carslaw et al*., 1995] increases by 30% with a 0.1°C temperature decrease. Comparing the measured temperature with threshold temperatures, T_{NAT}, T_{STS}, and T_{ICE}, helps determine the possible PSC particle types measured by the WLPC.

3. Antarctic Stratospheric Particle Observations

A summary of the first WLPC flight over the 6 days of measurements is shown in Figure 2. The track (Figure 2a) of the gondola indicates that it remained south of −76° latitude and passed near the South Pole. Measured particle number concentrations (Figure 2b) indicate continuous measurements of particles ≤ 0.25 μm with sporadic and random measurements of particles ≥ 0.46 μm. The measurements occurred primarily between T_{NAT} and T_{STS} with potential temperature nearly constant between 410 and 415 K (Figure 2c). High-frequency temperature variations are apparent and were measured by multiple thermistors: the two "Tsen" thermistors as well as two others located higher in the flight train. Similar measurements from multiple thermistors imply that these variations are real. They may result from gravity wave activity [*Hertzog et al*., 2008]. The measured pressure and density (Figure 2d) indicate that the gondola remained on a nearly isopycnic surface with variations in pressure < 2–3 hPa and density < 2–3 g m^{-3} throughout the flight. The high-frequency temperature fluctuations are reflected in the potential temperatures shown (Figure 2c). The variation of potential temperature throughout the 5 day flight was < 10 K, and < 5 K in the last 4 days, providing reasonable assurance of an instrument following an air mass. Air motions may also not be perfectly isentropic.

For a more complete picture of the temperature history of the air parcels sampled between 9 and 14 September, both isentropic and 3-D back trajectories were calculated using the Hybrid Single-Particle Lagrangian Integrated Trajectory (HYSPLIT) model developed by the NOAA Air Resource Laboratory [*Draxler and Rolph*, 2012]. Figure 3 shows the HYSPLIT isentropic back trajectories and air parcel temperature histories. The Global Data Assimilation System model was used within HYSPLIT which showed a

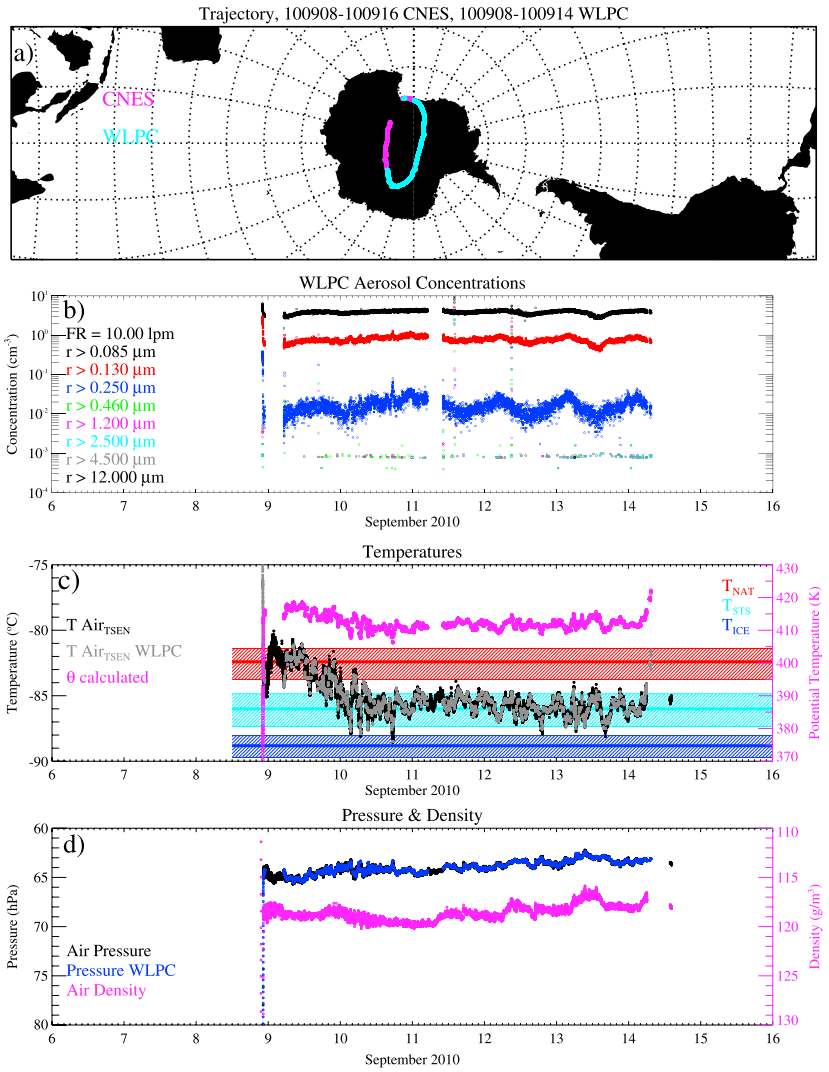

Figure 2. Measurements from WLPC flight from 100908 to 100914. (a) Position of the balloon obtained from the French Space Agency, CNES (pink), overwritten with the WLPC, position when WLPC was sampling (cyan). Temporal history of the measurements of the following: (b) particle concentrations with postflight test result channel boundaries listed on the left, starting with WLPC flow rate. (c) Temperature (black) and temperature during WLPC sampling (gray). Average threshold temperatures are indicated by colored horizontal lines labeled at the upper right with shading indicating uncertainty due to uncertainty of MLS mixing ratios of H_2O and HNO_3. Calculated potential temperature (pink) indicated by right *y* axis. (d) Air pressure (black) and pressure while WLPC was sampling (blue). Air density values (pink) are indicated by the right *y* axis.

warm bias of 1.5°C compared to observations. For the comparison shown, this bias was subtracted from the HYSPLIT temperatures.

The HYSPLIT back trajectories are similar to the gondola trajectories, although there are deviations from the gondola track, up to 300 km, as time increases along the back trajectory. To test this further, forward trajectories were performed for the first few days of the flight and compared with the gondola position. The calculated trajectories deviated from the gondola trajectory by an average of ~30 (maximum 60) km/d. These results are similar to the analysis of *Boccara et al.* [2008] who analyzed the trajectories of smaller superpressure balloons released from McMurdo in 2005. *Boccara et al.* [2008] show that after several days, simulated trajectories differ from balloon trajectories by several hundred kilometers even when isopycnic trajectories, i.e., mimicking the balloon behavior, were used. Given the errors and unresolved motions in analyzed winds, the difference between modeled and actual trajectory shown in Figure 3a is at least, or perhaps, more likely to result from errors in the analyzed winds used to construct the models, than it is to deviations of the gondola from a quasi-Lagrangian trajectory. The small variations in potential temperature (~1%) along the trajectory are also consistent with a quasi-Lagrangian trajectory.

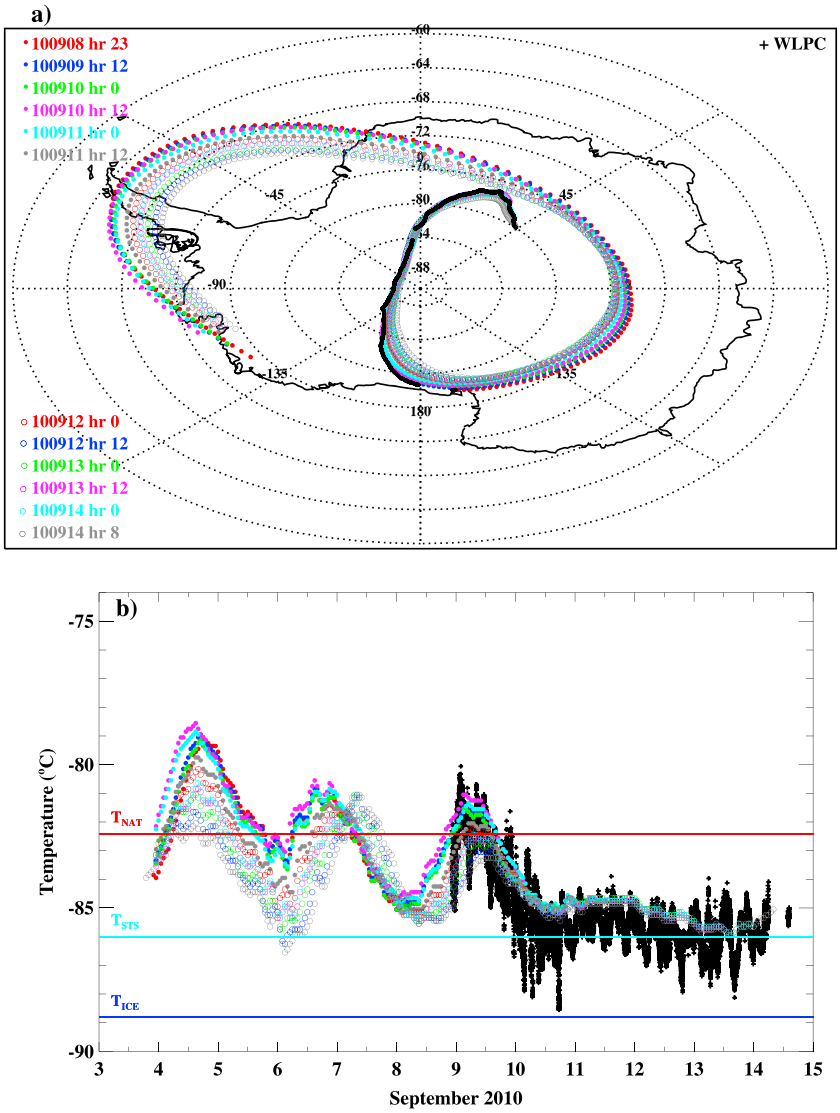

Figure 3. HYSPLIT isentropic back trajectories initialized for each 12 h of the WLPC flight. (a) Tracks over Antarctica of the WLPC and air parcel trajectories intersecting the balloon trajectory. Colored filled and open circles represent the back trajectories with starting points shown on the left. Black crosses indicate the track of the WLPC. (b) Day versus bias-corrected temperature from all HYSPLIT trajectories (same color scheme as Figure 3a) with observed temperature as black crosses. Average threshold temperatures are colored horizontal lines labeled on the left using H_2O and HNO_3 vapor concentration from MLS.

As the balloon reached its float altitude, the air parcel temperatures were primarily above T_{NAT}, Figure 3b, suggesting that initially the air may have been devoid of PSC particles. This conclusion must remain somewhat uncertain since, although the locus of initial measured temperatures were above T_{NAT} for about 12 h, and no NAT-like volumes were observed until 50 h later, the difference with T_{NAT} is small and some trajectory temperatures remained below T_{NAT}. In addition, at these temperatures, and supposing a saturation ratio for NAT of 0.5, it would take more than 12 h to evaporate a 0.5 μm particle [*Peter et al.*, 1994]. After this initial warm period, the air parcel temperature cooled within about a day to 2–3°C below T_{NAT} and remained at temperatures about 1°C warmer than T_{STS} for the next 4 days, until contact with the instrument was lost. Temperature histories from the 3-D trajectories (not shown) were warmer, by ~ 1°C, than the isentropic bias-corrected temperatures at the point where the gondola reached its float altitude; they then settled to match the isentropic temperatures within the next couple days of the flight.

Late in the day on 10 September the temperature approached T_{ICE}; however, all particles measured during this coldest period were less than 0.46 μm indicating that temperatures were not cold enough to initiate ice

formation. To induce homogeneous freezing temperatures roughly 3°C below T_{ICE} are required [*Koop et al*., 2000]. HYSPLIT temperatures, observed temperatures, and particle concentrations are all consistent with the conclusion that temperatures throughout the sampling period remained above T_{ICE}. While the coldest temperatures occurred on 10 September, high-frequency temperature fluctuations on the order of 2–3°C persisted, suggesting frequent excursions below T_{STS} although the majority of measurements were about 0.5°C warmer than T_{STS}, and well below T_{NAT}. These cold temperature measurements were investigated for the presence of STS, which would be reflected in particle growth, but none was found.

3.1. Determining Particle Phase

Without a direct measurement of particle phase, the type of observed particles is inferred by comparing model volumes for NAT, STS, and ice with volumes derived from the particle measurements. NAT and ice model volumes were found by comparing MLS HNO_3 and H_2O mixing ratios with saturation mixing ratios of HNO_3 over NAT [*Hanson and Mauersberger*, 1988] and of H_2O over ice [*Marti and Mauersberger*, 1993] as a function of temperature. The differences in mixing ratios represent the condensed gas and can be converted to volume. STS model volumes were calculated following *Carslaw et al*. [1995].

Total measured particle volumes were determined by fitting lognormal size distributions to WLPC particle measurements, allowing either a unimodal or bimodal fit [*Deshler et al*., 2003b]. For these fits the total number concentration of the distribution, N_o, was determined from condensation nuclei counter profile measurements on 29 August 2010 and 24 September 2010 from McMurdo [*Campbell and Deshler*, 2013]. Both profiles showed concentrations of ~10 cm^{-3} at the WLPC float altitude. With N_o measured, a unimodal distribution can be determined with two additional size-resolved concentration measurements, whereas a bimodal distribution requires five additional size-resolved concentration measurements. The lognormal distribution parameters were determined by minimizing the root-mean-square error between the logarithm of the fitted distribution and the measurements.

Three categories of size distribution fits to the observations were found, Figure 4. Over 5000 individual measurements resulted in lognormal fits similar to background stratospheric aerosol, with the largest particles measured around 0.6 μm, Figure 4a. These background distributions comprised the majority of WLPC samples. Eight 10 s samples with broader distributions containing particles up to approximately 3 μm were fit with a bimodal distribution, with a second mode median radius of 0.6 μm (Figure 4b). This broader first mode distribution and relatively small second mode median radius suggest growth of particles without a nucleation barrier. Similar distributions have been observed in the Arctic [*Schreiner et al*., 2003; *Deshler et al*., 2003a] and the Antarctic [*Del Negro et al*., 1997] where the particles were identified as STS. The third category contained 77 measurements with a second mode median radius > 2.0 μm, indicating growth of particles with a nucleation barrier [*Frenkel*, 1955]. Since temperatures remained warmer than T_{ICE} throughout the WLPC flight, these particle measurements are indicative of NAT. Of the 77 NAT distributions, 45 had a second mode that extended to particles as large as 5 μm (Figure 4c) while 32 distributions extended past 5 μm (Figure 4d). The average of total volumes for the background aerosol distributions was less than 0.04 $\mu m^3\ cm^{-3}$ while PSC particle volumes averaged $> 0.1\ \mu m^3\ cm^{-3}$.

Total volume measurements compared to PSC model volumes separated by flight day are shown in Figure 5. The range of modeled PSC volume reflects the MLS uncertainties in gas phase mixing ratios which were held constant for this analysis, as would be expected for a Lagrangian measurement. Figure 5 shows the dominance of background volumes for each day of the WLPC flight, while most volumes larger than background did not occur until the third day; two days after temperatures fell below T_{NAT}. Ten second samples consistent with NAT represented $< 1\%$ of the total number of samples. The decrease in gas phase HNO_3 due to uptake by such a small fraction of NAT is ~0.03 ppbv, which is well below the 0.7 ppbv uncertainty in the MLS HNO_3 measurement.

The first indication of observed volumes larger than background is shown on 11 September (Figure 5c); although, four out of five of these volumes were larger than any of the PSC models. The four 10 s measurements at −86°C all occurred within the first minute of one 2 min sampling period and had STS-like size distributions. These four distributions are included in the average distributions in Figure 4b. These larger volumes are a mystery. Perhaps they result from a narrow pocket of highly saturated air occurring due to massive denitrification from above, but this cannot be tested. Sedimentation from a PSC above, with quite

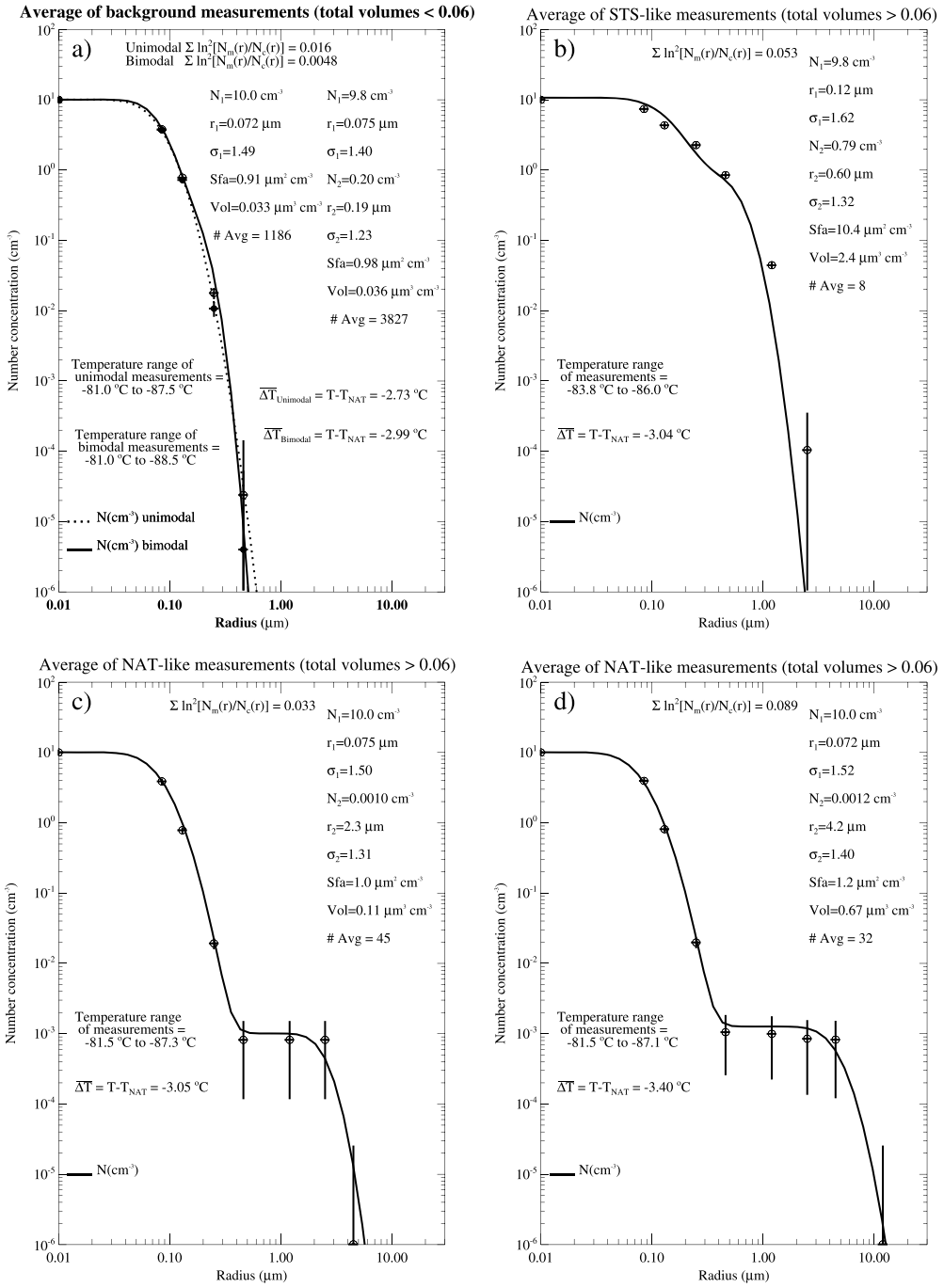

Figure 4. Average cumulative number concentration, both measured and fitted, versus radius, with the average fitting parameters listed on the right for the following: (a) Measurements consistent with stratospheric background aerosol, both unimodal (dotted line) and bimodal (solid line) seen throughout the whole flight. (b) Measurements with a relatively small second mode median radius, indicative of STS, mostly seen on 11 September. (c and d) Measurements with relatively large second mode median radius, indicative of NAT, mostly seen on 11–14 September. Number of measurements averaged listed below fit parameters on the right of each plot. The average root-mean-square error is listed at the top of each plot. The average cooling below T_{NAT} is on the bottom left. The horizontal error bars are difficult to see, but represent sizing uncertainty of 10%. The vertical error bars are concentration error bars and depend on Poisson counting statistics, thus increase at low concentrations, small counts. At high concentrations these error bars are difficult to separate from the data point.

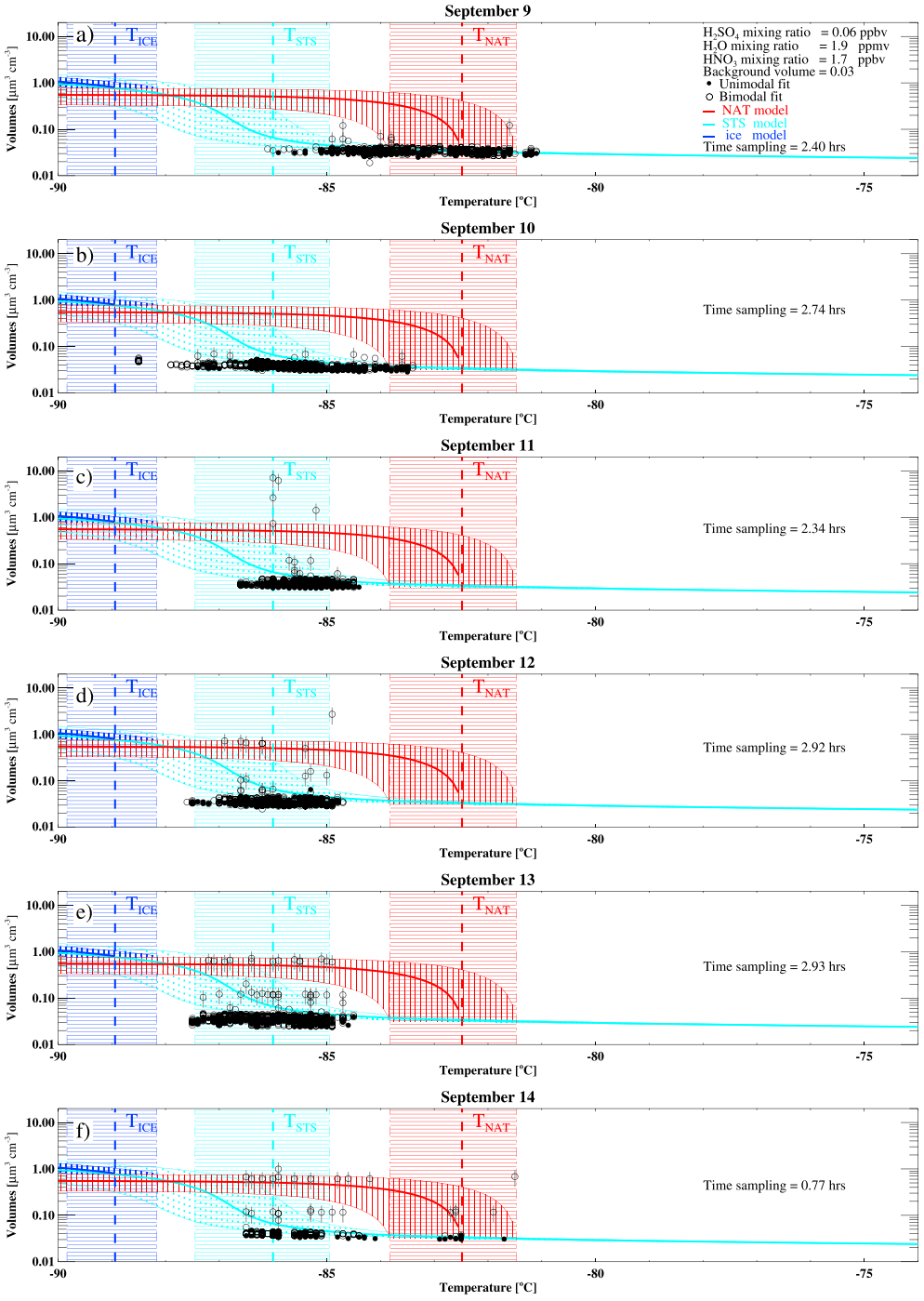

Figure 5. Modeled and measured volumes versus temperature for each day of the WLPC observations. Dashed vertical lines represent threshold temperatures labeled on the top next to dashed lines with shading around them showing MLS data uncertainty. Colored curves are NAT, STS, and ice modeled growth, labeled in the upper right. The lines surrounding curves represent each model's range due to MLS mixing ratio measurement uncertainty. Closed and open circles are measurements with unimodal and bimodal size distribution fits. Vertical lines through circles show ± 40% uncertainty of volumes. Each plot is a different day from (a–f) 9 September through 14 September. The amount of time samples taken for each day is listed on the right side of each plot. Average MLS measurements of H_2O and HNO_3 closest to the gondola are given in Figure 5a and are used in estimating the model PSC volumes.

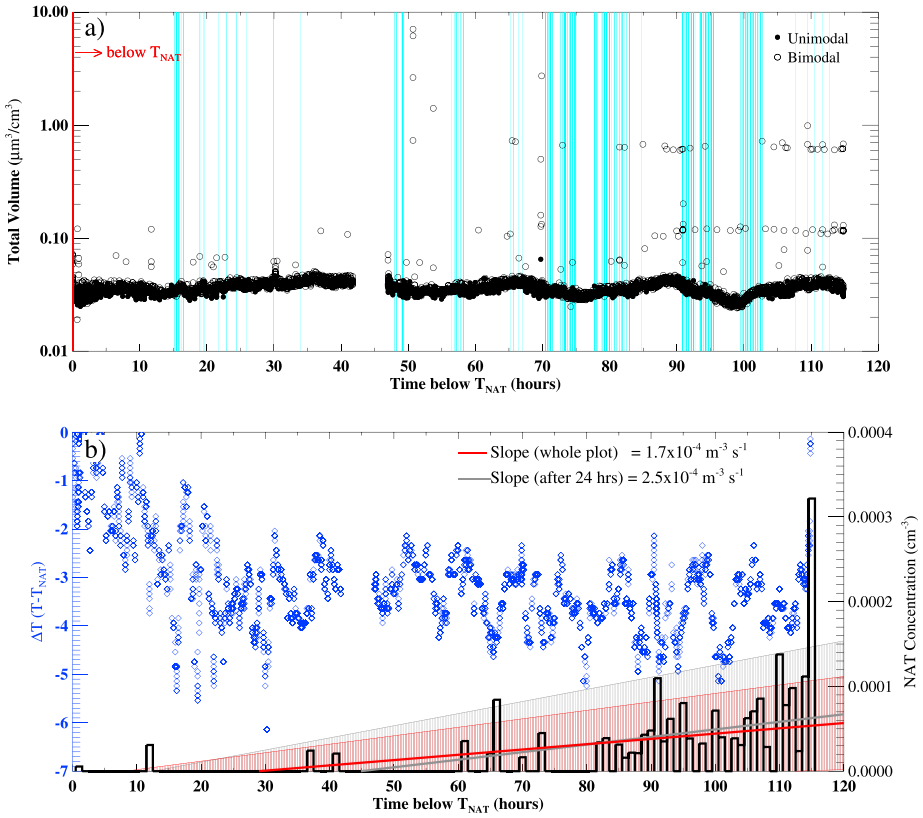

Figure 6. (a) WLPC estimates of total particle volume versus time below T_{NAT}. Unimodal fits to the particle measurements are closed circles and bimodal fits are open circles. Vertical cyan lines indicate measurements with temperatures below T_{STS}. No time was spent below T_{ICE}. (b) Amount of time below T_{NAT} versus number of particles in the second mode when volumes were between 0.08 and 1.0 μm^3 cm^{-3} over the total air volume measured in 1 h bins. Two lines are fit with one including the whole time period (solid red line) and one after 24 h below T_{NAT} when a stable temperature difference was reached (solid gray line). Uncertainty of the nucleation rates is ± 60% shown by the shaded region around each line with one standard deviation (1×10^{-4} m^{-3} s^{-1}) shown. Temperature below T_{NAT} is plotted with blue diamonds using the right *y* axis.

a different character from the gondola measurements is also unlikely. The Global Forecast System (GFS) was used to analyze temperatures above the gondola, and along back trajectories before the flight. These indicate that the coldest temperatures above the gondola were only ~2°C colder than those measured at the gondola around 17 km. Temperatures at 50–30 hPa were ~2°C above T_{NAT} on 5 September, and temperatures at these upper levels did not go below 1°C colder than T_{STS} through the rest of the flight. NAT particle sedimentation to the flight altitude is thus possible; however, STS or ice particles are unlikely. Assuming particle sizes similar to those measured, sedimentation would have been limited to 30–90 m above the gondola for the two previous days of the flight. This close to the gondola, these particles must have formed similarly to those at the WLPC altitude. Thus, the upper level temperature structure does not help explain the large particles. They remain a mystery.

After 11 September, each day showed an increasing number of observed volumes that fit the model of NAT growing to its equilibrium size or volumes below NAT but consistent with STS (Figures 5d–5f). *Larsen et al.* [1997] investigated temperature histories of PSCs observed from balloon-borne profile measurements and concluded that 1–2 days at temperatures colder than T_{NAT} are required for NAT to form. WLPC findings match those of *Larsen et al.* [1997] as 2 days of measurements below T_{NAT} occurred before volumes larger than background levels were observed.

3.2. Determining NAT Nucleation Rate

The increase in NAT-like volumes with longer time span below T_{NAT} suggests that the development of NAT PSCs has a time component which is analyzed in Figure 6. Approximately 50 h below T_{NAT} were observed by the WLPC prior to measurements of volumes > 0.2 μm^3 cm^{-3}, shown in Figure 6a. Evident in Figures 6, 5e,

and 5f are two issues which need to be addressed. The first is the bifurcation in the estimates of measured volume for particles above the background aerosol. There are observations of volumes slightly > 0.1 and then near 0.7 $\mu m^3\,cm^{-3}$. This bifurcation is reflective of the poor size resolution of the instrument. The measurements produce the lower volumes when the largest particle sensed is between 2.5 and 4.5 μm, thus triggering the 2.5 μm channel. The upper volumes arise when a particle between 4.5 and 12 μm is sensed and triggers the 4.5 μm channel. If the size resolution was finer at the large sizes, a more continuous distribution of volumes between 0.1 and 0.7 $\mu m^3\,cm^{-3}$ would be observed.

The second is the spatial and temporal discontinuity in the PSC measurements, which decreased with time. Between measurements consistent with PSCs there are many observations devoid of PSC particles. It is unknown why there is so much discontinuity in air that should contain PSCs. This is a surprise and does not fit with current understanding of PSCs. While it is impossible to rule out instrument error, or contamination on a remote drifting gondola, the fact that all measurements, with the exception of four, fit well within the realm of possible size distributions for PSCs and stratospheric aerosol, that the instrument was sensitive to all particle sizes throughout the measurement cycle, and that it performed as expected in postflight tests, all lead to the conclusion that the discontinuities are real.

To obtain a nucleation rate from the measurements, the number of particles in the second mode from NAT-like volumes ($0.08\,\mu m^3\,cm^{-3} <$ volume measured $< 1.0\,\mu m^3\,cm^{-3}$) in a 1 h period were divided by the total air volume measured in that hour. These 1 h bins of NAT particles nucleated per air volume measured were plotted against time below T_{NAT} indicating an increase with time (Figure 6b). A nucleation rate for NAT is given by the slope of the line fit to the 1 h binned measurements. The measured nucleation rates calculated in this way are $1.7 \times 10^{-4}\,m^{-3}\,s^{-1}$ if all measurements below T_{NAT} are used, or $2.5 \times 10^{-4}\,m^{-3}\,s^{-1}$ if only measurements at 3°C below T_{NAT}, when the temperature stabilized, are used.

The derived nucleation rates depend on the concentration of the second mode, N_2, when a NAT-like volume is observed. Uncertainties for the nucleation rate are found by estimating the uncertainty in determining N_2, which can be estimated as the fractional uncertainty in a concentration measurement [*Deshler et al.*, 2003b], which is $(NF/S)^{-1/2}$, where N is the concentration, F the flow rate (167 $cm^3\,s^{-1}$), and $S = 0.1$ Hz. From Figure 5 $N_2 = \sim 0.001\,cm^{-3}$, which results in an uncertainty of ± 80%. This value of N_2 is higher than the NAT concentration shown in Figure 6b because NAT concentration also accounts for all the air that was sampled which did not contain any large NAT particles. If a similar Poisson uncertainty is applied to the NAT concentrations of $\sim 0.0001\,cm^{-3}$, the uncertainty is ± 250%.

With these uncertainties in N_2 Monte Carlo simulations were used to provide a new temporal history of N_2, allowing each measurement of N_2 to randomly vary within ±80% or within ± 250% of the N_2 measured. For each simulation the slope, or nucleation rate, was recalculated. Since the errors are random, the average of the perturbed nucleation rates will not differ from those quoted above, but the distribution of nucleation rates around these averages provides an uncertainty on the slopes of the lines fit to the data in Figure 6b. The standard deviation of the Monte Carlo nucleation rates are ±15% and ± 45%, with the 95% confidence intervals at $\pm 6 \times 10^{-5}\,m^{-3}\,s^{-1}$, and $\pm 2 \times 10^{-4}\,m^{-3}\,s^{-1}$ for the two values of uncertainty in N_2. While this uncertainty range calculation is straight forward, given the uncertainties on N_2 and on the concentration of NAT, it does not reflect other uncertainties which are difficult or impossible to quantify, such as uncertainties in when the gondola cooled and stayed below T_{NAT}, the impact of intermittent sampling, and variations in exact air parcel temperature and vapor pressure history. For these reasons the uncertainty range shown in Figure 6b was taken as the sum of the two uncertainties on N_2, ± 60%.

Previous nucleation rates have been determined using temperature histories to find the time below T_{NAT} before a NAT PSC, or denitrification is observed, and then use microphysical models with varying nucleation rates to reproduce the measurement. A variety of such nucleation rates have been estimated. *Tabazadeh et al.* [2001] used modeled homogeneous freezing to indicate denitrification for one Antarctic and two Arctic winters and found an average NAT nucleation rate of $1 \times 10^{-3}\,m^{-3}\,s^{-1}$. Balloon-borne profile measurements of PSC particles over the Arctic from *Larsen et al.* [2004] resulted in a nucleation rate of $7 \times 10^{-3}\,m^{-3}\,s^{-1}$ for the air parcel, which cooled below T_{NAT} 1.75 days before measurement. *Grooß et al.* [2005] compared a chemical Lagrangian model to balloon-borne and research aircraft observations to obtain a nucleation rate of $2 \times 10^{-3}\,m^{-3}\,s^{-1}$ for Arctic early winter, January/early February, measurements. *Voigt et al.* [2005] found the same nucleation rate with research aircraft observations in the Arctic. A smaller nucleation rate of $8 \times 10^{-4}\,m^{-3}\,s^{-1}$ was determined with

Improved Limb Atmospheric Sounder satellite vapor measurements and ER-2 aircraft NO_y and particle measurements for the entire winter, while a balloon profile and MLS HNO_3 data were matched better with a higher nucleation rate of $3 \times 10^{-3}\,m^{-3}\,s^{-1}$ [*Davies et al*., 2005]. When considering late winter measurements, *Grooβ et al*. [2005] found a nucleation rate of $9 \times 10^{-4}\,m^{-3}\,s^{-1}$ matched March observations, which is lower than the early winter nucleation rate.

Even the smallest nucleation rate found with previous measurements is almost 4 times greater than that found with the quasi-Lagrangian WLPC measurements. These are two main differences between previous nucleation rates and the WLPC measurements. (1) All previous nucleation rate calculations, except the one Antarctic winter averaged with two Arctic winters considered by *Tabazadeh et al*. [2001], are over the Arctic and were in nondehydrated, nondenitrified conditions. The WLPC measurements were over Antarctica and within dehydrated and denitrified conditions. (2) Previous estimates of NAT nucleation rate used model temperature histories for the time below T_{NAT} before the particle concentration or denitrification was observed. The WLPC floated with the air parcel starting just before the parcel cooled below T_{NAT}. These measurements allowed particles to be measured as they appeared in the air parcel. Therefore, the WLPC observations provided the first direct measurement of a NAT nucleation rate, rather than determining one through fitting short-term observations using a microphysical parcel model.

NAT nucleation rates will depend on the degree of supercooling below T_{NAT}, on the concentration of heterogeneous NAT nuclei, and on the presence of extreme temperature fluctuations. The importance of these cannot be determined with these measurements. There are only a few degrees of supercooling between T_{NAT} and T_{STS}. For these quasi-Lagrangian measurements there is a slight to nonexistent trend in the temperature offset below T_{NAT} between 20 and 120 h after the temperature falls below T_{NAT}, Figure 6. The concentration of heterogeneous NAT nuclei, if they exist, will decrease through winter as NAT particles fall to lower altitudes. The loss of heterogeneous NAT nuclei would cause the NAT nucleation rate to decrease over the winter. The WLPC measurements occurred only at the end of the winter. The temperature fluctuations experienced were not large enough to cause nucleation from large supercooling. Another complication for the inferred nucleation rates could be sedimentation of large particles; however, there is a limited range above the gondola where NAT could have nucleated and fallen to the sampling altitude. Such particles would primarily be exposed to similar conditions as the gondola, so contamination from these particles is expected to be low and if present would lower the nucleation rate inferred. Finally, the accuracy of the measured nucleation rate is tempered slightly by the extent to which the flight trajectory deviated from a Lagrangian trajectory.

The measurements here indicate that when the observed particle volumes are consistent with NAT, the amount of particle growth is at the limit of what the HNO_3 vapor would provide in equilibrium, thus implying no growth barrier to NAT when it has formed. But the observations also suggest that NAT clouds can have a very sparse nature, even when conditions are favorable for NAT. Thus, the common model assumption that once temperatures are cold enough for NAT to form, the NAT particles are grown to equilibrium, causing subsequent widespread denitrification, may be in error. This could lead to a high bias in modeled denitrification [*Davies et al*., 2005; *Feng et al*., 2011] since the spatial heterogeneity of NAT clouds implied by these measurements is not considered.

4. Conclusions

The joint French-United States Concordiasi project's release of long-duration superpressure balloons from McMurdo Station, Antarctica, in 2010, provided a platform for the study of PSC formation. Temperature and particle measurements from one of these superpressure balloons indicated a nearly ideal environment for observation of NAT formation.

GPS position and temperature measurements over 6 days along the isopycnic surface on which the balloon floated were consistent with the Lagrangian back trajectory HYSPLIT model (within measurement and back trajectory uncertainties) indicating the quasi-Lagrangian nature of the measurements. The instrumented gondola reached its float altitude in the stratosphere at temperatures warmer than T_{NAT}. The air then cooled in 24 h to 2–3°C colder than T_{NAT}, close to T_{STS} and above T_{ICE}, and then remained at this temperature for the next 100 h.

Particle measurements indicated the dominance of background size distributions throughout the measurement period. There were, however, 77 particle distribution measurements with a well-defined second mode.

These distributions had particle volumes in agreement with NAT model volumes [*Deshler et al*., 2003a] but were not observed until 2 days after the air temperature cooled below $T_{NAT.}$ The number of observed particle volumes near NAT model volumes then increased with time below T_{NAT}.

Using the number of particles in the second distribution mode, for NAT-like size distributions, as a surrogate for NAT particles, the change in the number of NAT particles observed over time was used to infer an observed NAT nucleation rate of approximately $2 \times 10^{-4}\,m^{-3}\,s^{-1} \pm 60\%$. This nucleation rate is approximately 4 times smaller than previous estimates inferred from matching microphysical models to short-term measurements in the boreal early winter. Reasons for such differences could be related to differences between Antarctic and Arctic measurements, differences between early and late winter observations, or differences between the results here, inferred directly from measurements, and previous estimates that use microphysical models to match theoretical particle estimates with short-term particle measurements [*Tabazadeh et al*., 2001; *Larsen et al*., 2004; *Grooβ et al*., 2005]. Last, there is some previous indication that the NAT nucleation rate may decrease throughout the winter [*Grooβ et al*., 2005] as denitrification from early season PSCs removes HNO_3 or heterogeneous NAT nuclei become rarer due to sedimentation of particles earlier in the season. Our measurements correspond to the late winter time period.

Acknowledgments

Concordiasi is an international project, supported by the following agencies: Météo-France, CNES, CNRS/INSU, NSF, NCAR, University of Wyoming, Purdue University, University of Colorado, the Alfred Wegener Institute, the Met Office, and ECMWF. The measurements by the University of Wyoming within Concordiasi were supported by the NSF under OPP award 0636946. Concordiasi also benefits from logistic or financial support of the operational polar agencies Institut Polaire Français Paul Emile Victor (IPEV), Programma Nazionale di Ricerche in Antartide (PNRA), United States Antarctic Program (USAP), and British Antarctic Survey (BAS), and from Baseline Surface Radiation Network (BSRN) measurements at Concordia. Concordiasi is part of the Observing System Research and Predictability Experiment–International Polar Year (THORPEX-IPY) cluster within the International Polar Year effort. The Concordia website can be found at www.cnrm.meteo.fr/concordiasi/. The authors gratefully acknowledge the NOAA Air Resources Laboratory (ARL) for the provision of the HYSPLIT transport and dispersion model available at http://ready.arl.noaa.gov and NASA's Jet Propulsion Laboratory for the measurements of water and nitric acid from the Earth Observing System Microwave Limb Sounder on the Aura satellite used in this publication.

References

Boccara, G., A. Hertzog, C. Basdevant, and F. Vial (2008), Accuracy of NCEP/NCAR reanalysis and ECMWF analyses in the lower stratosphere over Antarctica in 2005, *J. Geophys. Res.*, *113*, D20115, doi:10.1029/2008JD010116.

Campbell, P. C., and T. Deshler (2013), Condensation nuclei measurements in the mid-latitude (1982–2012) and Antarctic (1986–2010) stratosphere between 20 and 35 km, *J. Geophys. Res. Atmos.*, doi:10.1002/2013JD019710, in press.

Carslaw, K. S., B. P. Luo, S. L. Clegg, T. Peter, P. Brimblecombe, and P. J. Crutzen (1994), Stratospheric aerosol growth and HNO_3 and water uptake by liquid particles, *Geophys. Res. Lett.*, *21*, 2479–2482.

Carslaw, K. S., B. P. Luo, and T. Peter (1995), An analytic expression for the composition of aqueous HNO_3-H_2SO_4 stratospheric aerosols including gas phase removal of HNO_3, *Geophys. Res. Lett.*, *22*, 1877–1880.

Carslaw, K. S., M. Wirth, A. Tsias, B. P. Luo, A. Dörnbrack, M. Leutbecher, H. Volkery, W. Renger, J. T. Bacmeister, and T. Peter (1998), Particle microphysics and chemistry in remotely observed mountain polar stratospheric clouds, *J. Geophys. Res.*, *103*, 5785–5796.

Crutzen, P. J., and F. Arnold (1986), Nitric acid cloud formation in the cold Antarctic stratosphere: A major cause for the springtime "ozone hole", *Nature*, *324*, 651–655.

Davies, S., G. W. Mann, K. S. Carslaw, M. P. Chipperfield, J. A. Kettleborough, M. L. Santee, H. Oelhaf, G. Wetzel, Y. Sasano, and T. Sugita (2005), 3-D microphysical model studies of Arctic denitrification: Comparison with observations, *Atmos. Chem. Phys.*, *5*, 3093–3109, doi:10.5194/acp-5-3093-2005.

Del Negro, L. A., et al. (1997), Evaluating the role of NAT, NAD, and liquid H_2SO_4/H_2O/HNO_3 solutions in Antarctic polar stratospheric cloud aerosol: Observations and implications, *J. Geophys. Res.*, *102*, 13,255–13,282.

Deshler, T., B. Nardi, A. Adriani, F. Cairo, G. Hansen, F. Fierli, A. Hauchecorne, and L. Pulvirenti (2000), Determining the index of refraction of polar stratospheric clouds above Andoya (69°N) by combining size-resolved concentration and optical scattering measurements, *J. Geophys. Res.*, *105*, 3943–3953.

Deshler, T., et al. (2003a), Large nitric acid particles at the top of an Antarctic stratospheric cloud, *J. Geophys. Res.*, *108*(D16), 4517, doi:10.1029/2003JD003479.

Deshler, T., M. E. Hervig, D. J. Hofmann, J. M. Rosen, and J. B. Liley (2003b), Thirty years of in situ stratospheric aerosol size distribution measurements from Laramie, Wyoming (41°N), using balloon-borne instruments, *J. Geophys. Res.*, *108*(D5), 4167, doi:10.1029/2002JD002514.

Draxler, R. R., and G. D. Rolph (2012), HYSPLIT (HYbrid Single-Particle Lagrangian Integrated Trajectory) model, NOAA Air Resources Laboratory, Silver Spring, Md., access via NOAA ARL READY Website (http://ready.arl.noaa.gov/HYSPLIT.php).

Dye, J. E., B. W. Gandrud, D. Baumgardner, K. R. Chan, G. V. Ferry, M. Loewenstein, K. K. Kelly, and J. C. Wilson (1990), Observed particle evolution in the polar stratospheric cloud of January 24, 1989, *Geophys. Res. Lett.*, *17*, 413–416.

Dye, J. E., D. Baumgardner, B. W. Gandrud, S. R. Kawa, K. K. Kelly, M. Loewenstein, G. V. Ferry, K. R. Chan, and B. L. Gary (1992), Particle size distributions in Arctic polar stratospheric clouds, growth and freezing of sulfuric acid droplets, and implications for cloud formation, *J. Geophys. Res.*, *97*, 8015–8034.

Dye, J. E., et al. (1996), In-situ observations of an Antarctic polar stratospheric cloud: similarities with Artic observations, *Geophys. Res. Lett.*, *23*, 1913–1916.

Fahey, D. W., et al. (2001), The detection of large HNO_3-containing particles in the winter Arctic stratosphere, *Science*, *291*, 1026–1031.

Farman, J. C., B. G. Gardiner, and J. D. Shanklin (1985), Large losses of total ozone in Antarctica reveal seasonal ClO_x/NO_x interaction, *Nature*, *315*, 207–310.

Feng, W., M. P. Chipperfield, S. Davies, G. W. Mann, K. S. Carslaw, S. Dhomse, L. Harvey, C. Randall, and M. L. Santee (2011), Modelling the effect of denitrification on polar ozone depletion for Arctic winter 2004/2005, *Atmos. Chem. Phys.*, *11*, 6559–6573, doi:10.5194/acp-11-6559-2011.

Frenkel, J. (1955), *Kinetic Theory of Liquids*, Dover, Mineola, N.Y.

Fueglistaler, S., B. P. Luo, C. Voigt, K. S. Carslaw, and T. Peter (2002), NAT-rock formation by mother clouds: A microphysical model study, *Atmos. Chem. Phys.*, *2*, 93–98.

Glen, A. (2007), *A New Optical Particle Counter for in situ Measurements of Stratospheric Aerosol Size Distributions*, University of Wyoming, Laramie, Wyo.

Grooβ, J.-U., G. Günther, R. Müller, P. Konopka, S. Bausch, H. Schlager, C. Voigt, C. M. Volk, and G. C. Toon (2005), Simulation of denitrification and ozone loss for the Arctic winter 2002/2003, *Atmos. Chem. Phys.*, *5*, 1437–1448, doi:10.5194/acp-5-1437-2005.

Hanson, D., and K. Mauersberger (1988), Laboratory studies of the nitric acid trihydrate: Implications for the south polar stratosphere, *Geophys. Res. Lett.*, *15*, 855–858.

Hertzog, A., C. Basdevant, F. Vial, and C. R. Mechoso (2004), The accuracy of stratospheric analyses in the Northern Hemisphere inferred from long-duration balloon flights, *Q. J. R. Meteorol. Soc.*, *130*, 607–626, doi:10.1256/qj.03.76.

Hertzog, A., et al. (2007), Stratéole/vorcore—Long-duration, superpressure balloons to study the Antarctic lower stratosphere during the 2005 winter, *J. Atmos. Oceanic Technol.*, *24*, 2048–2061, doi:10.1175/2007/JTECHA948.1.

Hertzog, A., G. Boccara, R. A. Vincent, F. Vial, and P. Cocquerez (2008), Estimation of gravity-wave momentum fluxes and phase speeds from quasi-Lagrangian stratospheric balloon flights. 2: Results from the Vorcore campaign in Antarctica, *J. Atmos. Sci.*, *65*, 3056–3070, doi:10.1175/2008JAS2710.1.

Hofmann, D. J., J. W. Harder, S. R. Rolf, and J. M. Rosen (1987), Balloon-borne observations of the development and vertical structure of the Antarctic ozone hole in 1986, *Nature*, *326*, 59–62.

Koop, T., U. M. Biermann, W. Raber, B. P. Luo, P. J. Crutzen, and T. Peter (1995), Do stratospheric aerosol droplets freeze above the ice frost point?, *Geophys. Res. Lett.*, *22*, 917–920.

Koop, T., K. S. Carslaw, and T. Peter (1997), Thermodynamic stability and phase transitions of PSC particles, *Geophys. Res. Lett.*, *24*, 2199–2292.

Koop, T., B. Luo, A. Tsias, and T. Peter (2000), Water activity as the determinant for homogeneous ice nucleation in aqueous solutions, *Nature*, *604*, 611–614, doi:10.1038/35020543.

Larsen, N., B. M. Knudsen, J. M. Rosen, N. T. Kjome, R. Neuber, and E. Kyro (1997), Temperature histories in liquid and solid polar stratospheric cloud formation, *J. Geophys. Res.*, *102*, 23,505–23,517.

Larsen, N., et al. (2004), Formation of solid particles in synoptic-scale Arctic PSCs in early winter 2002/2003, *Atmos. Chem. Phys.*, *4*, 2001–2013, doi:10.5194/acpd-4-2485-2004.

Livesey, N. J., et al. (2011), Earth Observing System (EOS) Microwave Limb Sounder (MLS) version 3.3 Level 2 data quality and description document, *Rep. JPL D-33509*, Jet Propulsion Laboratory, Pasadena, Calif.

Marti, J., and K. Mauersberger (1993), A survey and new measurements of ice vapor pressure at temperatures between 170 and 250 K, *Geophys. Res. Lett.*, *20*, 363–366.

McCormick, M. P., H. M. Steele, P. Hamil, W. P. Chu, and T. J. Swissler (1982), Polar stratospheric cloud sightings by SAM II, *J. Atmos. Sci.*, *39*, 1387–1397.

Middlebrook, A. M., L. T. Iraci, L. S. McNeill, B. G. Koehler, M. A. Wilson, O. W. Saastad, M. A. Tolbert, and D. R. Hanson (1993), Fourier transform-infrared studies of thin H_2SO_4/H_2O films: Formation, water uptake, and solid-liquid phase changes, *J. Geophys. Res.*, *98*, 20,473–20,481.

Peter, T., R. Muller, P. J. Crutzen, and T. Deshler (1994), The lifetime of leewave-induced ice particles in the Artic stratosphere: II. Stabilization due to NAT-coating, *Geophys. Res. Lett.*, *21*, 1331–1334.

Pitts, M. C., L. R. Poole, A. Dörnbrack, and L. W. Thomason (2011), The 2009–2010 Arctic polar stratospheric cloud season: A CALIPSO perspective, *Atmos. Chem. Phys.*, *11*, 2161–2177, doi:10.5194/acp-11-2161-2011.

Poole, L. R., and M. P. McCormick (1988), Airborne lidar observations of Arctic polar stratospheric clouds: Indications of two distinct growth stages, *Geophys. Res. Lett.*, *15*, 21–23.

Poole, L. R., M. T. Osborn, and W. H. Hunt (1988), Lidar observations of Arctic polar stratospheric clouds, 1988: Signature of small, solid particles above the frost point, *Geophys. Res. Lett.*, *15*, 867–870.

Pueschel, R. F., et al. (1989), Condensed nitrate, sulfate, and chloride in Antarctic stratospheric aerosols, *Geophys. Res. Lett.*, *94*, 11,271–11,284.

Rabier, F., et al. (2013), The Concordiasi field experiment over Antarctica: First results from innovative atmospheric measurements, *Bull. Am. Meteorol. Soc.*, *94*, ES17–ES20, doi:10.1175/BAMS-D-12-00005.1.

Schreiner, J., et al. (2003), Chemical, microphysical, and optical properties of polar stratospheric clouds, *J. Geophys. Res.*, *107*(D5), 8313, doi:10.1029/2001JD000825.

Solomon, S., R. R. Garcia, F. S. Rowland, and D. J. Wuebbles (1986), On the depletion of Antarctic ozone, *Nature*, *321*, 755–758.

Stanford, J. L., and J. S. Davis (1974), A century of stratospheric cloud reports: 1870–1972, *Bull. Am. Meteorol. Soc.*, *55*, 213–219.

Tabazadeh, A., R. P. Turco, K. Drbla, M. Z. Jacobson, and O. B. Toon (1994), A study of type I polar stratospheric cloud formation, *Geophys. Res. Lett.*, *21*, 1619–1622.

Tabazadeh, A., E. J. Jensen, O. B. Toon, K. Drdle, and M. R. Schoeberl (2001), Role of the stratospheric polar freezing belt in denitrification, *Science*, *291*, 2591–2594.

Toon, O. B., P. Hamill, R. P. Turco, and J. Pinto (1986), Condensation of HNO_3 and HCl in the winter polar stratosphere, *Geophys. Res. Lett.*, *13*, 1284–1287.

Voigt, C., et al. (2000), Nitric acid trihydrate (NAT) in polar stratospheric cloud particles, *Science*, *290*, 1756–1758.

Voigt, C., et al. (2005), Nitric acid trihydrate (NAT) formation at low NAT supersaturation in polar stratospheric clouds (PSCs), *Atmos. Chem. Phys.*, *5*, 1371–1380, doi:10.5194/acp-5-1371-2005.

Zhang, R., M.-T. Leu, and M. J. Molina (1996), Formation of polar stratospheric clouds on preactivated background aerosols, *Geophys. Res. Lett.*, *23*, 1669–1672.